



Three-dimensional measurements of traveling ionospheric disturbances with the Poker Flat Incoherent Scatter Radar

Michael J. Nicolls¹ and Craig J. Heinselman¹

Received 2 August 2007; revised 18 September 2007; accepted 1 October 2007; published 13 November 2007.

[1] In this paper, we present results from the Advanced Modular Incoherent Scatter Radar (AMISR) installed at the Poker Flat Research Range near Fairbanks, Alaska, the Poker Flat Incoherent Scatter Radar (PFISR), that focus on the ability of the system to make three-dimensional, simultaneous measurements of ionospheric parameters. We present observations from PFISR where we were able to resolve the three components of the \mathbf{k} vector of a traveling ionospheric disturbance (TID), as well as the period. These measurements give insight into the atmospheric gravity wave (AGW)-TID relationship, allowing us to apply a recently developed dispersion relation for AGWs that includes the role of kinematic viscosity and thermal diffusivity, important effects in the upper atmosphere, without assumptions about horizontal wavelengths. The analysis indicates that for this particular case, the wave must have been propagating against a background wind of ~ 125 m/s. PFISR will be a powerful tool for studying the sources and propagation of waves in the upper atmosphere. **Citation:** Nicolls, M. J., and C. J. Heinselman (2007), Three-dimensional measurements of traveling ionospheric disturbances with the Poker Flat Incoherent Scatter Radar, *Geophys. Res. Lett.*, 34, L21104, doi:10.1029/2007GL031506.

1. Introduction

[2] Enhanced currents and heating in the auroral zone can set up large amplitude atmospheric gravity waves (AGWs), which propagate in the form of traveling atmospheric disturbances (TADs) in the lower thermosphere. TADs are manifested in the ionosphere as traveling ionospheric disturbances (TIDs) [Hines, 1960], and may be formed in the polar atmosphere through direct heat deposition from precipitating particles or fluctuations in the auroral electrojet. This latter mechanism leads to the dissipation of energy via Joule heating or Lorentz forcing, and is in general more important than the effects of precipitating particles [e.g., Hunsucker, 1982; Hocke and Schlegel, 1996]. However, the dominance of either the Joule or Lorentz mechanisms is not as clear [e.g., Chimonas and Hines, 1970]. Joule heating is generated via ionization in the auroral region causing enhanced conductivity in conjunction with electric fields of magnetospheric origin. In the Lorentz case, electric fields set the plasma into motion and this momentum is transferred into the neutral atmosphere through collisions, causing intense wind surges and neutral heating through viscous

forcing. Waves produced by Joule heating may be more effective in propagating to low latitudes [e.g., Richmond, 1979], although other results suggest that the Lorentz term is more dominant except in very active storm-time conditions [Hunsucker, 1982]. Both mechanisms play an important role in the generation of AGWs in the auroral zone. In addition, tropospheric sources are also important at all latitudes, and may be the dominant source of medium-scale TIDs.

[3] Most observations of AGWs in the F region are made indirectly through measurements of TIDs in the electron density or ion velocity, although some studies have focussed on TIDs in other ionospheric parameters [e.g., Kirchengast, 1996]. However, a major shortcoming is the inability to measure all relevant TID properties. For example, a single vertically looking radar can measure the vertical wavelength of the TID/AGW. The period can also be measured using the variation of the perturbations as a function of time. However, a dispersion relation (e.g., that of Hines [1960]) must then be used to relate the observed perturbations to a horizontal wavelength and phase velocity. Such predictions can be validated using multiple instruments spaced in latitude/longitude, which complicates the interpretation of any study. Exceptions to “single-point” measurements include those made by the SuperDARN network of HF radars [e.g., Bristow *et al.*, 1994, 1996; Bristow and Greenwald, 1996] where the effects of AGWs are observed over an extended horizontal area by sensing the focussing/defocussing of ground-backscattered radiowaves and those made by the MU radar in Japan [e.g., Oliver *et al.*, 1994, 1996, 1997], which is able to investigate the three-dimensional characteristics of propagating waves using pulse-to-pulse steering.

[4] AMISR technology circumvents some of the difficulties in AGW measurements by allowing for the extraction of all the relevant properties of TIDs, including horizontal and vertical wavelengths and propagation directions. Such measurements could be very powerful in the study of the generation of AGWs/TIDs in the high latitude region and the redistribution of momentum and energy from the auroral region to lower latitudes. Here, we use such observations to investigate a recently developed dispersion relation for AGW [Vadas and Fritts, 2005] that explicitly accounts for the role of viscosity and thermal diffusivity, important effects in the thermosphere.

2. Experiment Description

[5] The Poker Flat Incoherent Scatter Radar (PFISR) is located at the Poker Flat Research Range (65.13°N, 147.47°W) near Fairbanks, Alaska. PFISR is a phased array allowing for pulse-to-pulse steering, providing a powerful extension over typical ISR approaches, which offer high

¹Center for Geospace Studies, SRI International, Menlo Park, California, USA.

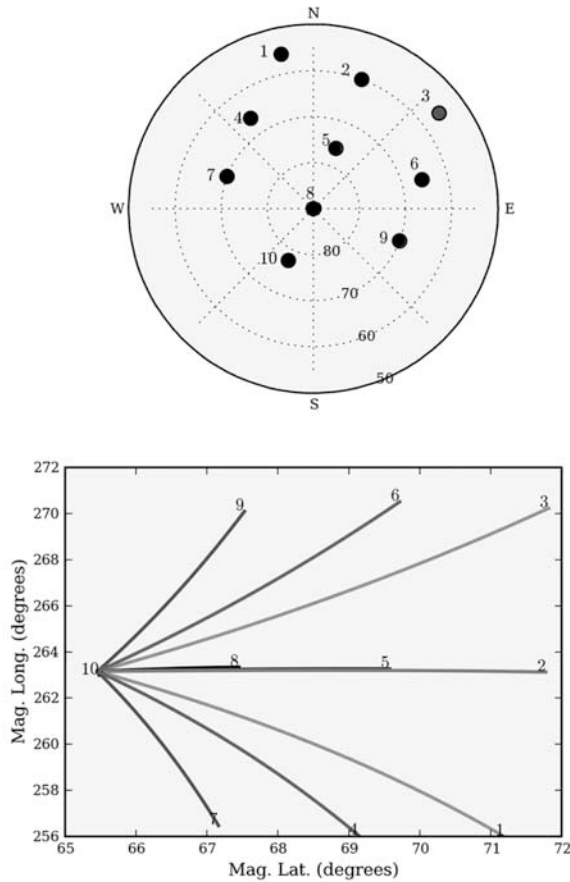


Figure 1. (top) Look directions of the 10 beams. (bottom) Geomagnetic latitude and longitude coverage of the beams out to 1000 km range.

resolution measurements in one direction only, or reduced time resolution in multiple directions through physical steering. The radar itself is tilted so that its boresight direction corresponds to elevation and azimuth angles of 74° and 15° . Figure 1 shows the geometry for this experiment. The azimuth and elevation of the beam positions are indicated, as well as the magnetic latitude-longitude coverage out to 1000 km range. The experimental configuration employed 10 beam positions, including three pairs spread in magnetic latitude, three pointed along the magnetic meridian, and one pointed up the magnetic field line. This experimental configuration is useful for electric field and ionospheric-parameter measurements close to zenith, although more latitudinal coverage is possible using beams with lower elevation angles. The dip angle varies from beam to beam, but is in the range of 75° – 85° in the F region.

[6] The experimental mode consisted of transmitting long pulses ($480 \mu\text{s}$, corresponding to 72 km of range smearing) for F -region measurements on two frequencies (449.6 and 449.3 MHz) separated by 300 kHz to best use the available 10% duty cycle of the system. The total power of the 96-panel PFISR system is about 1.3 MW. Samples were taken every $30 \mu\text{s}$ (4.5 km). About 10 seconds of data (~ 66 pulses per direction per frequency) were averaged together, then

one minute of data were combined with a median (total accumulation of ~ 792 pulses per direction).

3. Results

[7] Plotted in Figure 2 are the PFISR density measurements on December 13, 2006 from all beams. The densities have been calibrated using daytime plasma line measurements, but do not include a T_e/T_i correction needed to obtain absolute density [e.g., Evans, 1969]. There are clear fluctuations in the densities, particularly evident on the bottom-side, possibly associated with AGWs. To investigate this possibility, in Figure 3 we plot an estimate of the density perturbations, $\delta N_e/N_e$, which is computed by filtering the densities in Figure 2. Clear evidence of AGW signatures can be seen as periodic density perturbations with amplitudes near ± 10 – 15% in all beams with a period near 20–25 minutes. The wave amplitudes maximize on the bottom-side and the altitude extent varies with time but generally reaches at least 240 km. We note that density perturbations with varying periods and wavelengths have been observed in many daytime F -region measurements made with PFISR. The high occurrence rate is not too surprising since there is a seasonal dependence of TID observations at high latitudes that peaks in the wintertime with a high detection probability close to 80% [Bristow *et al.*, 1996]. Waves have also been observed with very high occurrence rates at other locations, especially Arecibo [Djuth *et al.*, 2004].

[8] The perturbations show clear downward phase progression, a requirement for an upward propagating AGW [Hines, 1960]. The density perturbations themselves are caused by the AGW winds dragging the plasma along the field line, leading to periodic plasma advection and compression/rarefaction [Hooke, 1970]. Diffusion and recombination may also play a role in determining the fluctuation level. The density perturbations are expected to be $\sim 90^\circ$ out of phase with the AGW wind perturbations. Velocity perturbations (not shown), in the range ± 20 m/s, confirm our interpretations (see examples in a companion paper, S. Vadas and M. J. Nicolls, Using PFISR measurements and gravity wave dissipative theory to determine the neutral, background thermospheric winds, submitted to *Geophysical Research Letters*, 2007, hereinafter referred to as Vadas and Nicolls, submitted manuscript, 2007). With these effects evident in the data, it is very likely that the perturbations are the result of upward propagating waves. The contours of the electron density perturbations are somewhat curved with increasing altitude, often indicating an “S-like” shape. A changing vertical wavelength with altitude may be the result of changing atmospheric conditions, such as viscosity or neutral winds. Of course, temperature effects (scale height and buoyancy frequency) also change with altitude.

[9] The advantages of PFISR over traditional TID measurements should be clear; with simultaneous multi-position measurements, it should be possible to extract the horizontal wavelengths of the wave. Measurements of the density perturbations as a function of time from any range and look direction can be compared with the measurements from another beam, giving an estimate of the wave \mathbf{k} vector between the two points. A particular measurement i corresponds to $\mathbf{A}_i \cdot \mathbf{k}/m = y_i$ where \mathbf{k} is a vector representing the AGW wavenumber, integer m represents an inherent 2π

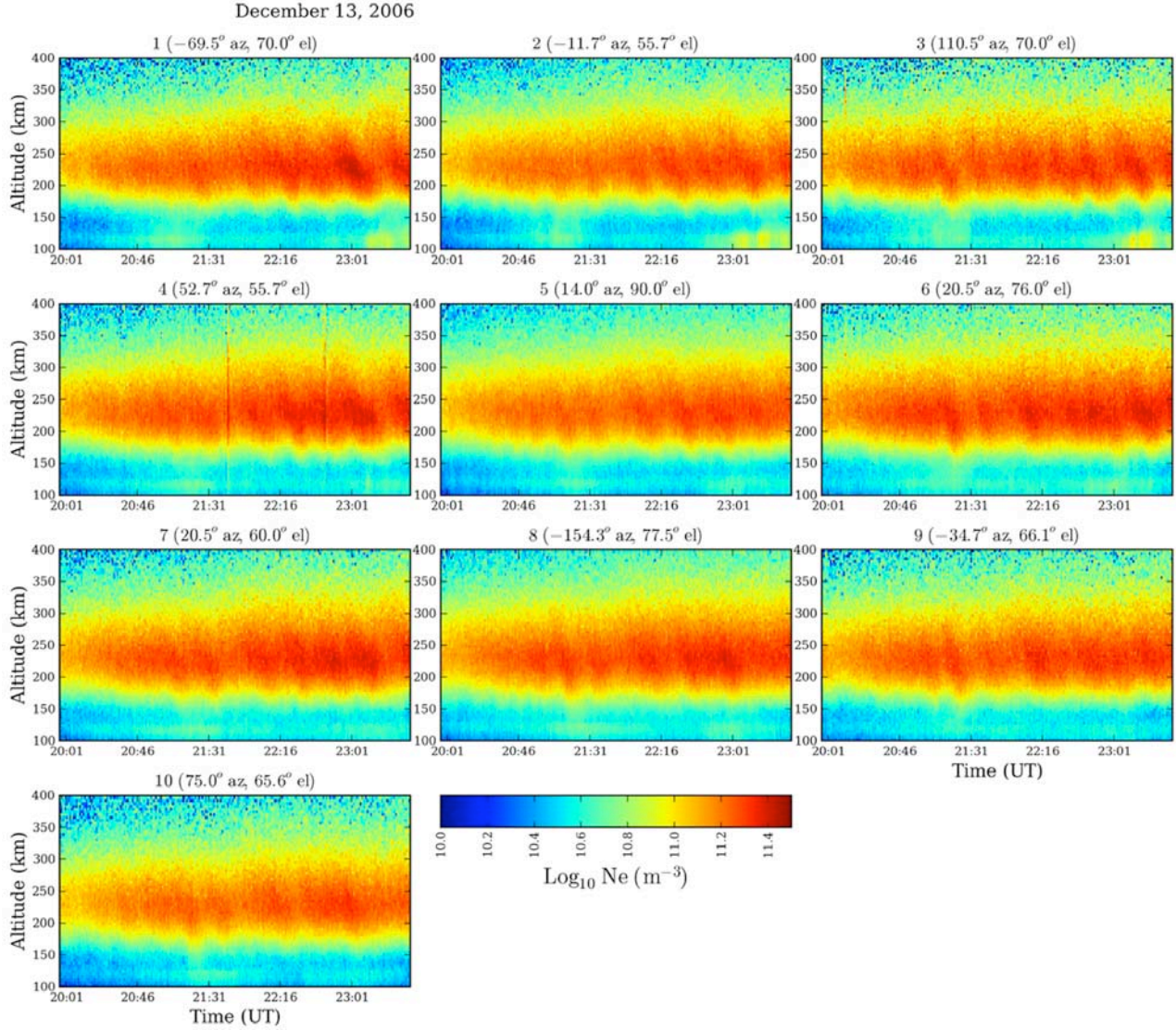


Figure 2. Raw electron densities (no T_e/T_i correction) measured with the 10 beams on 12/13/2006.

ambiguity (spatial aliasing), \mathbf{A}_i is a vector of geometrical scale factors equal to the vector between the two measurements ($\mathbf{A}_i = R_1^i \hat{\mathbf{a}}_1 - R_2^i \hat{\mathbf{a}}_2$ where R_1^i and R_2^i are the ranges and $\hat{\mathbf{a}}_1$ and $\hat{\mathbf{a}}_2$ are unit observation vectors of the two beams; in geographic coordinates (north, east, up), $\hat{\mathbf{a}}_j = [\cos \phi_j \cos \theta_j, \cos \phi_j \sin \theta_j, \sin \phi_j]$ where ϕ_j and θ_j are the elevation and azimuth angles of beam j), and y_i is the measurement (in this case the phase delay in radians, or $y_i = 2\pi \delta t / \tau$ where δt is the measured time delay and τ is the period of the wave). In matrix form, the system of n measurements can be represented as:

$$\begin{bmatrix} A_{1x} & A_{1y} & A_{1z} \\ A_{2x} & A_{2y} & A_{2z} \\ \vdots & \vdots & \vdots \\ A_{nx} & A_{ny} & A_{nz} \end{bmatrix} \begin{bmatrix} k_x \\ k_y \\ k_z \end{bmatrix} = \begin{bmatrix} y_1 \\ y_2 \\ \vdots \\ y_n \end{bmatrix}. \quad (1)$$

The problem is then one of inverting the system for the wave \mathbf{k} vector, and can be solved using an inverse method. All the different possible correlations can be handled in this approach, which is a significant number if one treats each

altitude from each beam as a distinct measurement of the wave. Here we only include correlations between adjacent beams (to avoid any possible aliasing and other geometrical effects) and target k_x and k_y (the horizontal components of the wave \mathbf{k} vector) by computing the phase delay between pairs of beams at similar altitudes so that the third column of the \mathbf{A} matrix will be small. For an estimate of k_z , we also include correlations from different altitudes from the vertically pointed beam. The system is inverted using a minimum mean square error estimator based on casting the problem into a Bayesian linear model form. The approach used returns an estimate of the full covariance matrix of the system that can be used to assess sampling deficiencies in the experiment.

[10] The dominant period of the wave and the phase delay between any two beams, y_i , was estimated using the complex cross-spectrum of the two time series near the estimated period of the AGW. We focus on the time period from about 2200–2330 UT where three clear wave periods were observed in all beams. The period of the wave was estimated to be $\tau = 22.3 \pm 1.1$ min, with the errorbar corresponding to the

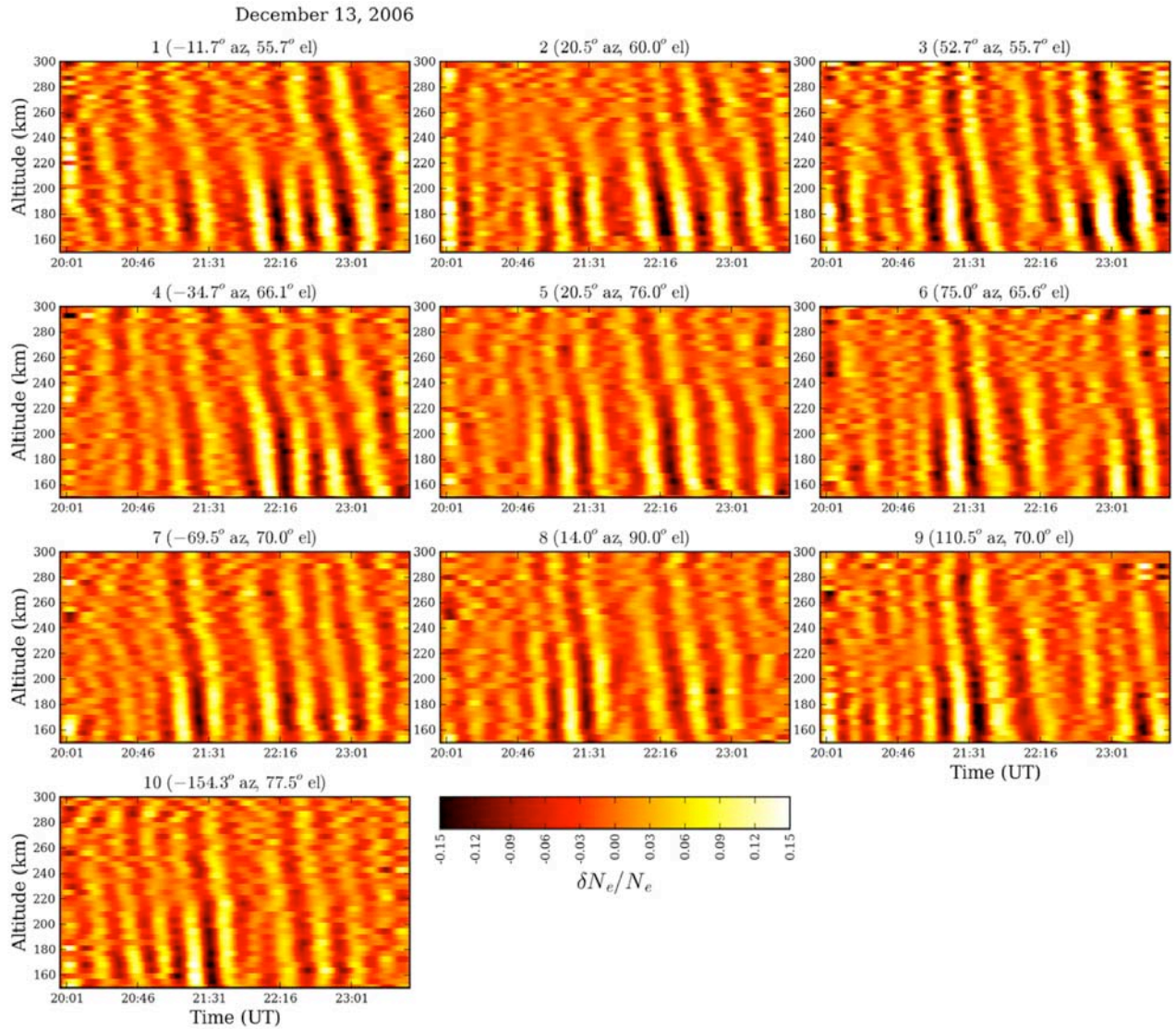


Figure 3. Density perturbation ($\delta N_e/N_e$) from all 10 beams.

standard deviation of the frequency estimates from all beam-to-beam cross spectra. Error estimates on the phase delays were included in the error covariance matrix provided to the inversion routine by examining the standard deviation of the phase angle over the -3-dB region around the spectral feature in the cross-spectral estimate. Applying the phase delays into the inversion approach described above (with a total of 18 beam pairs) from altitudes 160–220 km leads to horizontal wavelength estimates as a function of altitude. The median values and standard deviations of the estimates are: $\lambda_{north} = -216 \pm 12$ km and $\lambda_{east} = 373 \pm 28$ km with the horizontal wavelength components fairly constant with altitude, as expected. The horizontal wavelength estimate is then $\lambda_H = 187 \pm 8$ km.

[11] The method can also produce an estimate of the vertical wavelength, with the information coming from including correlations from adjacent altitudes from the same beam. For this experiment, we utilize only the vertically pointed beam for this determination, but this is not in general necessary. The median estimate for the vertical wavelength is $\lambda_z = -231.3 \pm 11.2$ km; however, it can be

observed that the vertical wavelength changes with altitude, which will be investigated in the next section. With these wavelengths and periods, the wave is observed to propagate in the southeastward direction (azimuth $\sim 150^\circ$) with horizontal phase velocity $v_\phi = 140 \pm 9$ m/s. The observed horizontal wavelength and propagation velocity place this TID into the medium-scale category [Hocke and Schlegel, 1996].

4. Discussion

[12] The classical non-dissipative AGW dispersion relation [Hines, 1960] leads to a prediction of the vertical wavenumber as,

$$k_z^2 \approx N^2 k_H^2 / \omega_I^2 - k_H^2 - 1/4H^2 \quad (2)$$

where $\omega_I = 2\pi/\tau - \mathbf{k} \cdot \mathbf{U}$ is the intrinsic frequency of the wave where \mathbf{U} is the neutral wind vector, N is the Brunt-Vaisala frequency, H denotes the atmospheric scale height,

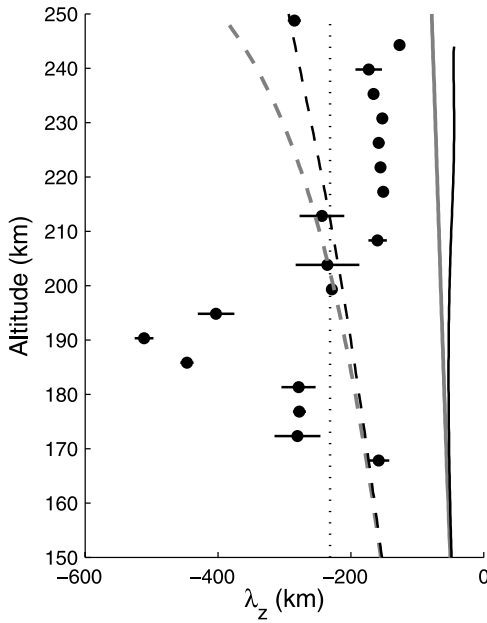


Figure 4. Vertical wavelength measurements (points with errorbars), prediction of equation 2 (gray), and prediction of equation 3 (black). The dashed curves includes a 125 m/s neutral wind against the wave. The vertical dotted line is the λ_z estimate from section 3.

and $k_H = \sqrt{k_x^2 + k_y^2} = 2\pi/\lambda_H$ is the horizontal wavenumber. In writing this anelastic dispersion relation, we have assumed that $\omega_i^2 \gg f_c^2$ where f_c is the Coriolis frequency and that $\omega_i/\sqrt{k^2 + 1/4H^2} < c_s$, where c_s is the acoustic speed. Both of these assumptions are valid for the AGW of interest. From equation 2, it is evident that the vertical wavelength is a function of altitude because of the changing atmospheric conditions - the variation of the winds as well as N (decreases with altitude) and H (increases with altitude).

[13] Equation 2 neglects all forms of dissipation, including viscosity (subsequently treated by *Pitteway and Hines* [1963]). Recently, an analytical dispersion relation has been formulated that includes the role of kinematic viscosity and thermal diffusivity explicitly, derived under the ansatz of a complex intrinsic frequency and real vertical wavenumber (instead of the classical approach of a real intrinsic frequency and a complex vertical wavenumber) [*Vadas and Fritts*, 2005]. That dispersion relation may be written in terms of the vertical wavenumber as [*Vadas and Fritts*, 2005; *Vadas*, 2007],

$$k_z^2 = \frac{N^2 k_H^2 \left\{ 1 + \frac{\nu^2}{4\omega_i^2} \left(k^2 - \frac{1}{4H^2} \right)^2 \frac{(1-Pr)^2}{[1+\delta(1+1/Pr)/2]^2} \right\}^{-1}}{\omega_i^2 [1 + \delta(1 + 1/Pr) + \delta^2/Pr]} - k_H^2 - \frac{1}{4H^2} \quad (3)$$

where k is the wavenumber magnitude; $\delta = \nu k_z/H\omega_i$; $Pr = 0.7$ is the Prandtl number (ratio of viscous to thermal diffusion); and ν is the kinematic viscosity. Note that δ is negative for an upward propagating wave and that equation 3 is recursive since the RHS depends on k_z through δ .

Equation 3 reduces to equation 2 if ν is set to 0. The dispersion relation can be evaluated using a model neutral atmosphere like MSIS, where the altitudinal variation of all terms is considered.

[14] Figure 4 shows a scatter plot of the AGW λ_z estimates as a function of altitude inferred using phase delays from different altitudes (separated by ~ 30 km) from the vertically pointed beam. The black dashed line is the estimate of λ_z quoted in the previous section. The solid gray and black curves are the vertical wavelengths predicted by equation 2 and equation 3, respectively, with the winds set to 0. While the *Hines* [1960] curve predicts a λ_z that increases continuously with altitude (because of the changing temperature), the *Vadas and Fritts* [2005] curve predicts that λ_z should peak at a value of 50–55 km near the dissipation altitude of the wave, about 180 km, and then decrease as the AGW perturbations become negligible. The measured λ_z , however, is much larger than the theory predicts assuming zero winds, especially at the lower altitudes, and also shows unexpected altitudinal variations. In Figure 3, between 2200 and 2300 UT, one sees λ_z increase at about 180 km (the slope of a $\delta N_e/N_e$ contour becomes larger) and then decrease again at higher altitudes. One possible explanation for a larger vertical wavelength than theory would suggest is that the wave is traveling against the wind, meaning that the intrinsic period of the wave is smaller than the ground-based period. A changing λ_z with altitude could be the result of a changing wind, modifying the intrinsic frequency of the AGW. To illustrate the effects of winds, the dashed curves show the λ_z resulting from a 125 m/s wind going against the wave.

[15] This suggests the possibility of using vertical wavelength estimates along with the *Vadas and Fritts* [2005] dispersion relation to estimate neutral winds as a function of altitude when AGW fluctuations are present. Such a measurement might provide a way to extract thermospheric zonal winds, which has been impossible with ISRs in the past. Meridional winds can be deduced using measurements of the parallel ion velocity. We emphasize that the winds can only be deduced in the direction of wave propagation. For more details on this approach, we refer the reader to a companion paper (*Vadas and Nicolls*, submitted manuscript, 2007).

5. Conclusion

[16] The multi-beam capability of PFISR has allowed us to investigate the three-dimensional properties of an MSTID. We have outlined a scheme to back out those properties by synthesizing measurements from multiple beams, casting the problem into a linear-model form. This approach will work even if the experimental geometry is not optimized for measurement of wave \mathbf{k} vectors (e.g., if no beam is pointed vertically), and thus we expect the method to be applicable to a variety of PFISR experiments. With these measurements, we were able to evaluate the AGW dispersion relation without assumption (other than neglecting background winds and utilizing a model neutral atmosphere). We compared the results to the *Vadas and Fritts* [2005] anelastic dispersion relation, which includes the effects of kinematic viscosity and thermal diffusion. To reconcile differences between the vertical wavelength from

theory and measurements, we postulate that the AGW is propagating against a background wind (intrinsic period smaller than ground-based period). These results indicate that PFISR will be a powerful tool for the study of upper atmospheric waves. With the three-dimensional measurements, the formation of AGWs, their relationship to TIDs, and their role in depositing and redistributing energy into the thermosphere and to lower latitudes can be investigated.

[17] **Acknowledgments.** The data collection and analysis for PFISR was supported under NSF cooperative agreement ATM-0608577. MJN would like to acknowledge Sharon Vadas for useful discussions and comments.

References

- Bristow, W. A., and R. A. Greenwald (1996), Multiradar observations of medium-scale acoustic gravity waves using the Super Dual Auroral Radar Network, *J. Geophys. Res.*, *101*(A11), 24,499–24,511.
- Bristow, W. A., R. A. Greenwald, and J. C. Samson (1994), Identification of high-latitude acoustic gravity wave sources using the Goose Bay HF radar, *J. Geophys. Res.*, *99*(A1), 319–331.
- Bristow, W. A., R. A. Greenwald, and J. P. Villain (1996), On the seasonal dependence of medium-scale atmospheric gravity waves in the upper atmosphere at high latitudes, *J. Geophys. Res.*, *101*(A7), 15,685–15,699.
- Chimonas, G., and C. O. Hines (1970), Atmospheric gravity waves launched by auroral currents, *Planet. Space Sci.*, *18*(4), 565–582.
- Djuth, F. T., M. P. Sulzer, S. A. Gonz ales, J. D. Mathews, J. H. Elder, and R. L. Walterscheid (2004), A continuum of gravity waves in the Arecibo thermosphere?, *Geophys. Res. Lett.*, *31*, L16801, doi:10.1029/2003GL019376.
- Evans, J. V. (1969), Theory and practice of ionosphere study by Thomson scatter radar, *Proc. IEEE*, *57*(4), 496–530.
- Hines, C. O. (1960), Internal atmospheric gravity waves at ionospheric heights, *Can. J. Phys.*, *38*, 1441–1481.
- Hocke, K., and K. Schlegel (1996), A review of atmospheric gravity waves and travelling ionospheric disturbances: 1982–1995, *Ann. Geophys.*, *14*(9), 917–940.
- Hooke, W. H. (1970), The ionospheric response to internal gravity waves, *J. Geophys. Res.*, *75*, 5535–5544.
- Hunsucker, R. D. (1982), Atmospheric gravity waves generated in the high-latitude ionosphere: A review, *Rev. Geophys.*, *20*(2), 293–315.
- Kirchengast, G. (1996), Elucidation of the physics of the gravity wave-TID relationship with the aid of theoretical simulations, *J. Geophys. Res.*, *101*(A6), 13,353–13,368.
- Oliver, W. L., S. Fukao, Y. Yamamoto, T. Takami, M. D. Yamanaka, M. Yamamoto, T. Nakamura, and T. Tsuda (1994), Middle and upper atmosphere radar observations of ionospheric density gradients produced by gravity wave packets, *J. Geophys. Res.*, *99*(A4), 6321–6329.
- Oliver, W. L., S. Fukao, M. Sato, Y. Otsuka, T. Takami, and T. Tsuda (1996), Middle and upper atmosphere radar observations of the dispersion relation for ionospheric gravity waves, *J. Geophys. Res.*, *100*(A12), 23,763–23,768.
- Oliver, W. L., Y. Otsuka, M. Sato, T. Takami, and S. Fukao (1997), A climatology of *F* region gravity wave propagation over the middle and upper atmosphere radar, *J. Geophys. Res.*, *102*(A7), 14,499–14,512.
- Pitteway, M. L. V., and C. O. Hines (1963), The viscous damping of atmospheric gravity waves, *Can. J. Phys.*, *41*, 1935–1948.
- Richmond, A. D. (1979), Large-amplitude gravity wave energy production and dissipation in the thermosphere, *J. Geophys. Res.*, *84*(A5), 1880–1890.
- Vadas, S. L. (2007), Horizontal and vertical propagation and dissipation of gravity waves in the thermosphere from lower atmospheric and thermospheric sources, *J. Geophys. Res.*, *112*, A06305, doi:10.1029/2006JA011845.
- Vadas, S. L., and D. C. Fritts (2005), Thermospheric responses to gravity waves: Influences of increasing viscosity and thermal diffusivity, *J. Geophys. Res.*, *110*, D15103, doi:10.1029/2004JD005574.

C. J. Heinselman and M. J. Nicolls, Center for Geospace Studies, SRI International, 333 Ravenswood Avenue, Menlo Park, CA 94025, USA. (craig.heinselman@sri.com; michael.nicolls@sri.com)